Effect of low temperature baking in nitrogen on the performance of a niobium superconducting radio frequency cavity

Pashupati Dhakal,[1] Santosh Chetri,[2] Shreyas Balachandran,[2] Peter J. Lee,[2] and Gianluigi Ciovati[1]

[1]*Thomas Jefferson National Accelerator Facility, Newport News, Virginia 23606, USA*
[2]*Applied Superconductivity Center, National High Magnetic Field Laboratory, Tallahassee, Florida 32310, USA*

(Received 10 November 2017; published 8 March 2018)

We report the rf performance of a single cell superconducting radiofrequency cavity after low temperature baking in a nitrogen environment. A significant increase in quality factor has been observed when the cavity was heat treated in the temperature range of 120–160 °C with a nitrogen partial pressure of ~25 m Torr. This increase in quality factor as well as the Q-rise phenomenon (anti-Q-slope) is similar to those previously obtained with high temperature nitrogen doping as well as titanium doping. In this study, a cavity N_2-treated at 120 °C and at 140 °C showed no degradation in accelerating gradient, however the accelerating gradient was reduced by ~25% with a 160 °C N_2 treatment, compared to the baseline tests after electropolishing. Sample coupons treated in the same conditions as the cavity were analyzed by scanning electron microscope, x-ray photoelectron spectroscopy and secondary ion mass spectroscopy revealed a complex surface composition of Nb_2O_5, NbO and $NbN_{(1-x)}O_x$ within the rf penetration depth. Furthermore, magnetization measurements showed no significant change on bulk superconducting properties.

DOI: 10.1103/PhysRevAccelBeams.21.032001

I. INTRODUCTION

Recent advances in the processing of bulk superconducting radio frequency (SRF) niobium cavities via interior surface impurity diffusion have resulted in significant improvements in their quality factor (Q_0). The motivation for the development of these processes is to reduce the cryogenic operating cost of current and future accelerators while providing reliable operation. The potential for higher Q_0 in SRF cavities was first realized by titanium doping [1–3] during high temperature annealing of SRF cavity at 1400 °C and later by nitrogen doping at 800 °C [4], followed by electropolishing (EP). "Titanium doping" is introduced during the annealing of a niobium cavity in a vacuum furnace in the presence of a titanium source at a temperature greater than 1200 °C, in order to achieve an adequate partial pressure of titanium for absorption into the Nb surface. "Nitrogen doping" consists in the annealing of a niobium cavity at 800 °C in the presence of a partial pressure of nitrogen of ~25 m Torr, which diffuses into the Nb surface (NbN precipitates are also produced on the surface which must be subsequently removed). The experimental results show that such "doping" processes not only resulted in an increase in quality factor at low field levels, but also an increase in quality factor with increasing accelerating gradient, contrary to the previously observed Q-slope. A possible explanation for the high quality factor is the trapping of hydrogen at interstitial sites due to the diffused atoms [5,6] and reduction on the formation of lossy hydrides during cavity cooldown [7]. A possible explanation for the Q-rise ("anti-Q-slope") phenomenon is related to the presence of sharper peaks in the electronic density of states at the gap edges in doped cavities and such peaks being broadened by the rf current [8,9]. However, despite the increase in Q_0, the quench field of the cavities doped by titanium or nitrogen is often limited to much lower values than achieved by standard treatments [3,10]. Even though no definitive cause is known, it is likely due to early vortex penetration due to the reduction of the lower critical field by material doping [11,12].

Results on SRF cavities which were heat treated in the temperature range of 800–1600 °C without subsequent chemical etching showed improvements in the quality factor compared to standard preparation methods by reducing mostly the Bardeen-Cooper-Schrieffer (BCS) surface resistance as well as the residual resistance, to a lesser extent [13,14]. Most recently, efforts have been made to preserve high accelerating gradients while also increasing the quality factor of SRF cavities [15,16]. In these new nitrogen "infusion" cavity processing recipes, cavities were

heat treated at 800 °C for 3 hours, then the furnace temperature is reduced to 120–200 °C and nitrogen is introduced into the furnace at a partial pressure of ~25 m Torr for ~48 h. This process has shown an improvement in Q_0 over the baseline measurements, without the need for postannealing chemical etching. Even though diffusion of the nitrogen into the bulk of the SRF cavity is limited in depth at these low temperatures (120–200 °C) [17], the introduction of nitrogen is sufficient to modify the cavity surface within the rf penetration depth as seen from rf results, which are similar to those previously reported for high-temperature nitrogen doped cavities. Furthermore, while postdoping electropolishing is required to remove coarse nitrides from the surfaces of high-temperature nitrogen doped cavities, no further processing is required for the low-temperature infusion recipe showing a clear benefit in reducing processing steps as well as keeping higher gradient with high Q_0 values. In this manuscript, we present the results from several rf tests on a single cell cavity treated in a low temperature nitrogen environment as well as analyses of sample coupons treated under similar conditions.

II. CAVITY SURFACE PREPARATION

One single cell cavity of low-loss shape (frequency = 1.5 GHz, geometric factor = 277.2 Ω, $E_p/E_{\mathrm{acc}} = 1.99$ and $B_p/E_{\mathrm{acc}} = 4.18$ mT/(MV/m)) was fabricated from high purity (RRR > 300) fine-grain Nb. The cavity fabrication followed the standard procedure of deep-drawing disks then machining of the iris and equator and finally electron beam welding the assembly. After the fabrication of the cavity, the interior was polished by standard electropolishing to remove ~150 μm from the inner surface of the cavity. The cavity was then subjected to high temperature degassing at 800 °C for 2 hours in a resistive vacuum furnace followed by the removal of 20 μm from the surface by electropolishing. The annealing temperature is measured by a thermocouple attached to a panel inside the hot zone. Standard procedures were followed to clean the cavity surface in preparation for an rf test: degreasing in ultrapure water with a detergent and ultrasonic agitation, high pressure rinsing with ultrapure water, drying in the ISO4/5 cleanroom, assembly of flanges with rf feedthroughs and pump out ports and evacuation. The cavity was inserted in a vertical cryostat and cooled to 4.5 K with liquid helium using the standard Jefferson Lab cool-down procedure in a residual magnetic field of <2 mG. This procedure results in a temperature difference between the two irises $\Delta T > 4$ K when the equator temperature crosses the superconducting transition temperature (~9.2 K), which provides good flux expulsion conditions [18]. Before the heat treatment, the cavity was high pressure rinsed and then dried in an ISO 4/5 cleanroom. While in the cleanroom, special caps made from niobium foils similar to those used in Ref. [15] were placed to cover the cavity flange openings. The cavity was then transported to the furnace inside a clean, sealed plastic bag. The vacuum heat treatment procedure started with the 800 °C/3 h degassing step followed by lowering the temperature to the (120–160 °C) range. The furnace is continuously pumped until the furnace reaches ~290 °C, at which point the nitrogen partial pressure is increased to ~25 m Torr by introducing high-purity (99.999%) nitrogen gas from a cylinder. Such pressure is then maintained without active pumping of the furnace enclosure. Once the temperature has fallen to the desired value (120–160 °C), which is within ~2 hours, the temperature is held for ~46 hours. Figure 1 shows the typical temperature and partial pressure of the gas measured during the heat treatment process.

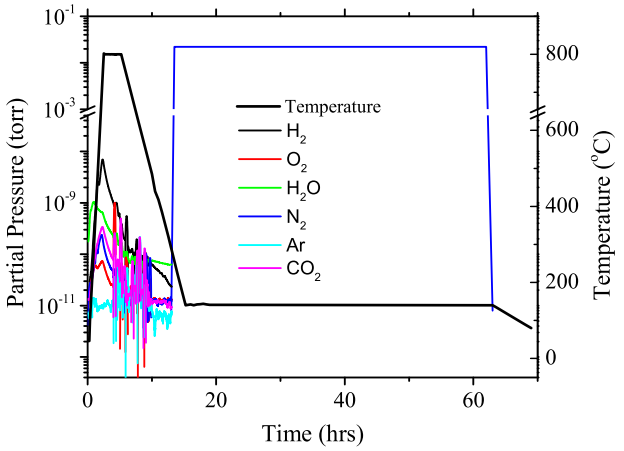

FIG. 1. Typical temperature and partial pressure of the gas measured during the heat treatment process. All partial pressures during the heat treatment were below 10^{-8} torr. The residual gas analyzer was turned off before N_2 injection.

After the heat treatment, the standard cavity cleaning procedures were applied before the rf test. After each heat treatment, the cavity's inner surface was reset (rf tests 4 and 6) with a standard ~10 μm EP. The sequential steps of cavity processing are as follows: (i) rf test 1; (ii) *in situ* 120 °C low temperature baking for 48 hours; (iii) rf test 2; (iv) HT at 800 °C/3 hrs followed by 120 °C/48 hrs in ~25 m Torr nitrogen; (v) rf test 3; (vi) ~10 μm standard electropolishing; (vii) rf test 4; (viii) HT at 800 °C/3 hrs followed by 160 °C/48 hrs in ~25 m Torr nitrogen; (ix) rf test 5; (x) ~10 μm standard electropolishing; (xi) rf test 6; (xii) HT at 800 °C/3 hrs followed by 140 °C/48 hrs in ~25 m Torr nitrogen; (xiii) rf test 7.

III. CAVITY RF RESULTS

The cavity immersed in the helium bath is excited using a phase-locked loop to measure the quality factor (surface resistance) as a function of temperature while the helium bath temperature was lowered by pumping down to ~1.5 K. The average rf surface resistance $R_s(T)$ was measured at low rf field ($B_p \sim 10$ mT) and fitted with the following equation:

$$R_s(T) = R_{\mathrm{BCS}}\left(T, \frac{\Delta}{K_B T_c}, l\right) + R_{\mathrm{res}}, \quad (1)$$

where R_{res} is the temperature independent residual resistance and R_{BCS} is BCS surface resistance. Here, Δ is the superconducting energy gap at 0 K, K_B is Boltzmann's constant, T_c is critical temperature, and l is the normal-electrons' mean free path. The BCS resistance was calculated using a computer program to solve Mattis-Bardeen equations to calculate the surface impedance at microwave frequency from the BCS theory of superconductivity [19,20] with parameters $T_c = 9.2$ K, London penetration depth $(\lambda_L) = 32$ nm and coherence length $(\xi_0) = 39$ nm, considered to be material constants for superconducting niobium. Figure 2 shows the R_{res}, $\Delta/K_B T_C$ and l obtained from the fit of $R_s(T)$. The residual resistance is consistently ≤ 2 nΩ, except for test 2 when the cavity was subjected to low temperature baking (LTB) at 120 °C for 48 hours in vacuum. Although this increase in residual resistance and decrease in mean free path (mfp) has been typically observed in the past for LTB cavities [21], the explanation is still not resolved. The mfp after baseline EP treatments is significantly higher ($l \sim 150$ nm) than after LTB and nitrogen infusion ($l < 50$ nm) suggesting that the Nb surface within the rf penetration depth changes from "clean" to "dirty" limit. Measurements of $Q_0(B_p)$ were done at 2.0 K up to the maximum gradient as limited by either breakdown or high field Q-slope.

It should be emphasized that the Mattis-Bardeen equations had been derived considering the rf field as a perturbation to the quasiparticles' Hamiltonian and result in a surface resistance which is independent from the field amplitude. This is clearly not the case for either doped or "infused" Nb cavities, as shown in Fig. 3. Because of the measured strong field dependence of R_s beginning at low field, the value of the material parameters obtained by fitting $R_s(T)$ with Eq. (1) would depend from the field amplitude at which $R_s(T)$ was measured. Therefore, the values of mean free path shown in Fig. 2 should be considered as a qualitative indication that the LTB of N-infusion make the rf surface dirtier. To the authors' knowledge a theory which allows calculating $R_s(T, B_p)$ for different values of material parameters is yet to be developed.

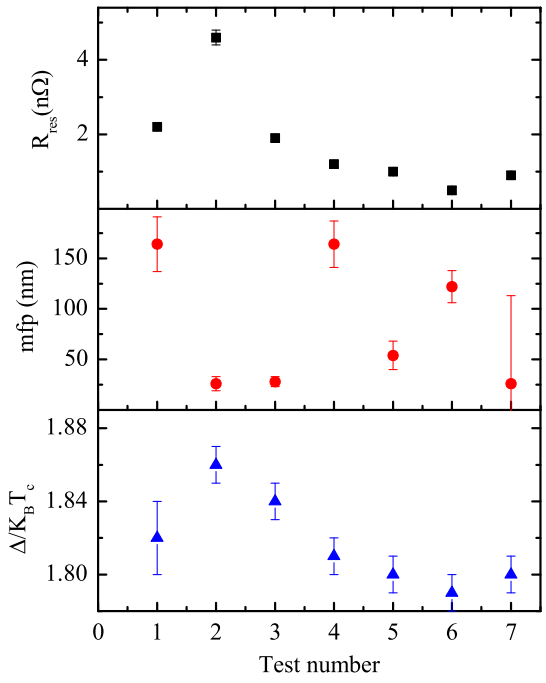

FIG. 2. Material parameters obtained from the fit of $R_s(T)$ from 4.3 to ~1.5 K. The error bars on some R_{res} values are within the size of the marker.

Figure 3(a) shows the $Q_0(E_{\mathrm{acc}})$ curve for the three baseline tests (tests 1, 4 and 6) measured at 2.0 K. All these three baseline tests have similar $Q_0(E_{\mathrm{acc}})$ dependence with small deviations above 30 MV/m, and all tests were limited by Q-slope without field emission. These results showed that ~10 μm surface removal by EP resets the surface such that a reproducible rf performance is achieved, regardless of the previous annealing. Figure 3(b) shows the $Q_0(E_{\mathrm{acc}})$ curves for the same cavity heat treated at different temperatures along with the baseline test 1. The cavity which received the LTB (test 2) at 120 °C for 48 hours on the vertical test stand after the baseline test 1 reached a maximum gradient of (46 ± 2) MV/m, which corresponds to a peak magnetic field of (196 ± 8) mT, close to the thermodynamic critical field of Nb at 2.0 K. As observed in the past, the Q-slope at high field is also minimized by the LTB at 120 °C for 48 hours done under ultrahigh vacuum (UHV) conditions. The cavity which was subjected to the additional 120 °C for 48 hours in a nitrogen partial pressure of ~25 m Torr showed no improvement in the accelerating gradient over the baseline electropolished cavity but a small increase in Q_0 (~20%) at all field levels. The improvement in Q_0 was not as high as recently reported on other cavities treated in a similar way [15], which may be due to not having a fresh electropolished surface prior to the furnace treatment or the nitrogen injection temperature being higher than that in Ref. [15]. We plan to explore the effect of surface conditions on cavity performances prior to the heat treatments in the future.

The cavity heat treated at 800 °C for 3 hours followed by 160 °C for 48 hours in nitrogen partial pressure of ~25 m Torr showed an improvement of Q_0 by a factor of ~2, with an extended Q-rise (reaching a maximum at ~16 MV/m) as observed in earlier nitrogen doped cavities at higher temperatures (800 °C) [3,4]. However, the cavity quenched at ~30 MV/m with a Q-slope starting at ~20 MV/m. The cavity heat treated at 800 °C for 3 hours followed by a 140 °C for 48 hours nitrogen infusion showed the best performance, with increasing Q_0 to a broad peak and a maximum accelerating gradient of ~39 MV/m, similar to the baseline tests. The Q-rise phenomenon is probably similar to the high temperature nitrogen doped cavities [8,9].

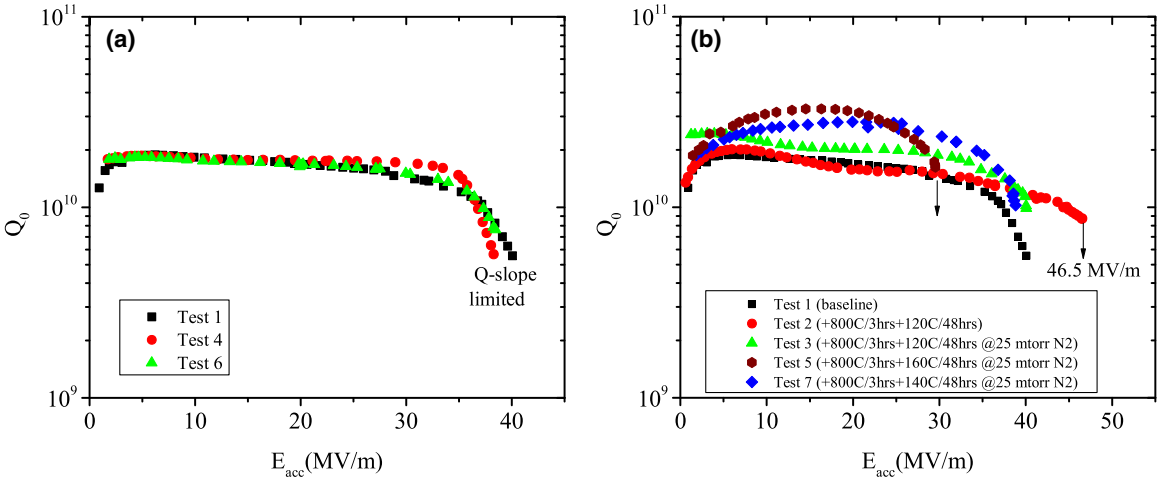

FIG. 3. Radio frequency measurement taken at 2.0 K for (a) the baseline measurements and (b) after different surface treatments.

IV. COUPON PREPARATION AND CHARACTERIZATION

Samples (7.5 mm × 5 mm × 3.125 mm in dimensions) labeled F9–F12 were cut by wire electrodischarge machining (EDM) from a high purity fine-grain niobium sheet. Cylindrical samples, (∼3 mm long, ∼1 mm diameter), labeled M8–M12 were cut by wire EDM from high purity Nb sheet (RRR > 300), BCP 1:1:1 to remove ∼100 μm. The samples F9–F12 were etched by BCP 1:1:1, removing ∼70 μm, heat treated in a UHV furnace at 600 °C for 10 hours to degas hydrogen, and etched by BCP 1:1:2, removing ∼30 μm. Afterwards, the samples were nanopolished at Wah Chang, USA, to obtain a surface with mirror quality smoothness. Another ∼20 μm BCP was done to remove any residue from the nanopolishing. Samples were heat treated at different temperature and environments as listed in Table I. The treatment of these samples attempted to replicate the cavity treatments as much as possible, most importantly the samples were heat treated inside an Nb tube enclosed by Nb caps to simulate the environment along with Nb cavity. The samples were analyzed by field emission scanning election microscopy (FESEM) to investigate the surface morphology and x-ray photoelectron spectroscopy (XPS) to identify the surface composition. Time of flight secondary ion mass spectroscopy (TOF-SIMS) was used for elemental information near the surface. The cylindrical samples were also heat treated along with the flat samples for dc magnetization measurement to determine the superconducting critical fields.

TABLE I. Summary of sample heat treatments.

Samples	Heat treatment	N_2 gas
M8	800 °C/3 h + 120 °C/48 h	···
F9, M9	800 °C/3 h	···
F10, M10	800 °C/3 h + 120 °C/48 h	∼25 m Torr
F11, M11	800 °C/3 h + 140 °C/48 h	∼25 m Torr
F12, M12	800 °C/3 h + 160 °C/48 h	∼25 m Torr

A. Surface morphology

Surface imaging was performed with a Zeiss 1540EsB FESEM. The polycrystalline macroscopic surface of the coupon samples after different surface treatments is shown at low magnification in Figs. 4(a)–(4d). FESEM backscattered electron (BSE) images, which are sensitive to crystallographic orientation and composition, show a mottled contrast, suggesting residual surface strains, on all samples irrespective of the heat treatment condition. The overall grain sizes in all samples are similar and in the range 20–100 μm, which is typical of fine-grain Nb sheets. There is no change in the macrograin structure after different low temperature nitrogen infusion heat treatments between 120–160 °C. Higher magnification BSE images of representative regions are shown in Figs. 5(a)–(5d). There is a clear difference in N-infused surfaces when compared with those annealed at the standard 800 °C/3 h in UHV. There is very weak in-grain surface channeling contrast in 800 °C/3 h, as shown in Fig. 5(a). All N-infused samples show surface structures as indicated by Figs. 5(b)–(5d). Studies are ongoing to clarify the nature of these features. There are two leading possibilities under consideration: (a) nitrogen infusion changes the surface composition leading to different morphologies of Nb oxides (mainly the outer layer of pentoxide), and (b) nanoscale niobium nitride islands. The density of the surface structures appears to increase with higher N-infusion temperature from 120 to 160 °C, although the density seems to depend on crystal orientation.

B. XPS results

For the XPS study (Physical Electronics PHI 5000 Series) the photoelectrons were excited using an x-ray source that produces MgK_α radiation at 1253.6 eV. Before acquiring the data, a very light sputtering was done using

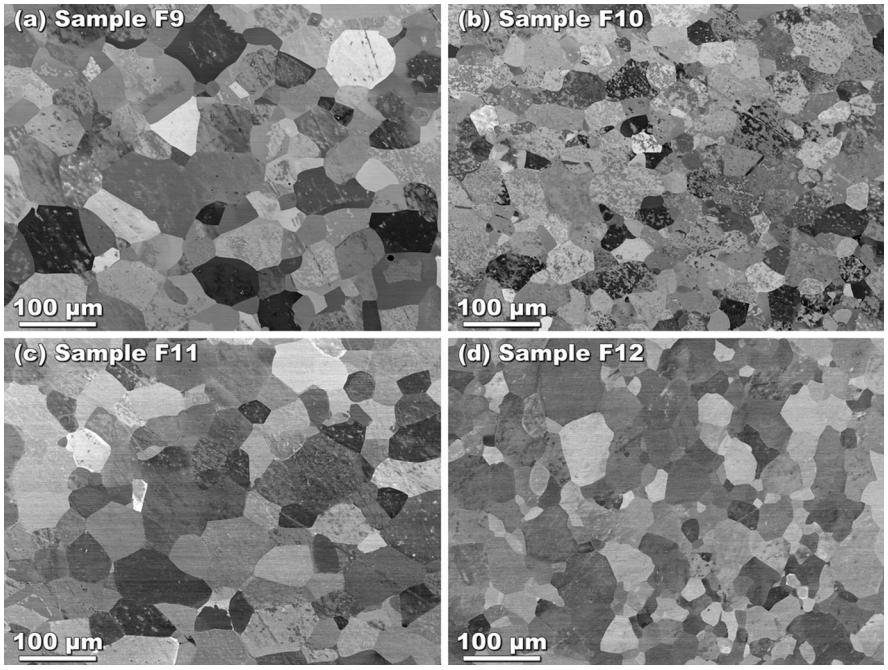

FIG. 4. Representative low magnification BSE images coupon sample surfaces with grain boundaries (GB) after different heat treatments, (a) 800 °C/3 h with no nitrogen infusion and (b)–(d) are low temperature nitrogen infused at 120, 140 and 160 °C, respectively.

1 μA argon ion at 3 keV just to remove any surface hydrocarbons. The data was acquired at different binding energy ranges for different elemental spectrum at a step size of 0.1 eV/step. The data was averaged among ten cycles. The electron energy analyzer was operated in a constant energy mode with pass energy 71.55 eV. For angle resolved XPS the data was taken at different takeoff angles: 15°, 30°, 45°, 60° and 75° (as the takeoff angle of photoelectrons is

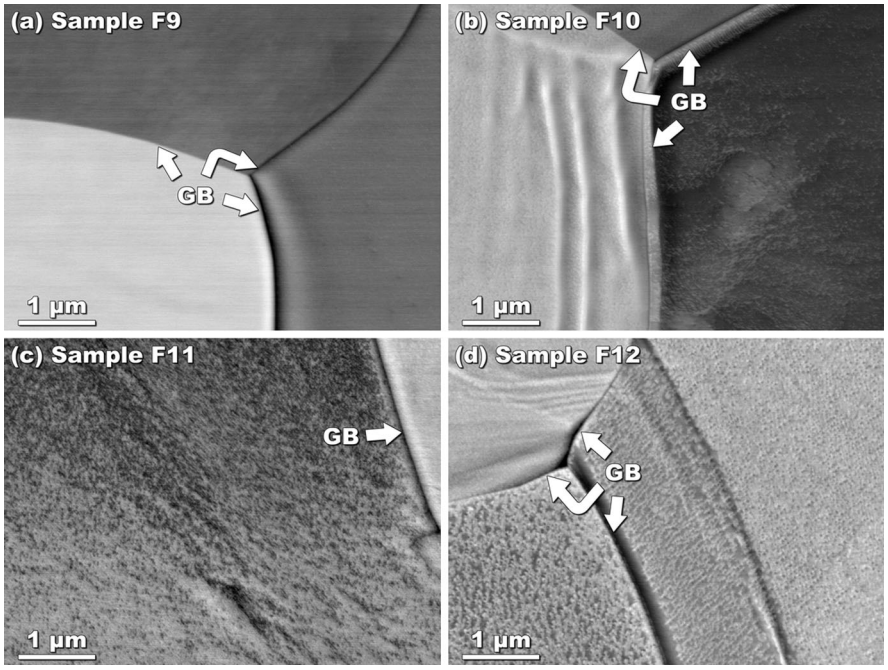

FIG. 5. Representative high magnification BSE image coupon sample surfaces with grain boundaries (GB) after different heat treatments, (a) 800 °C/3 h with no nitrogen infusion and (b)–(d) are low temperature nitrogen infused at 120, 140 and 160 °C, respectively.

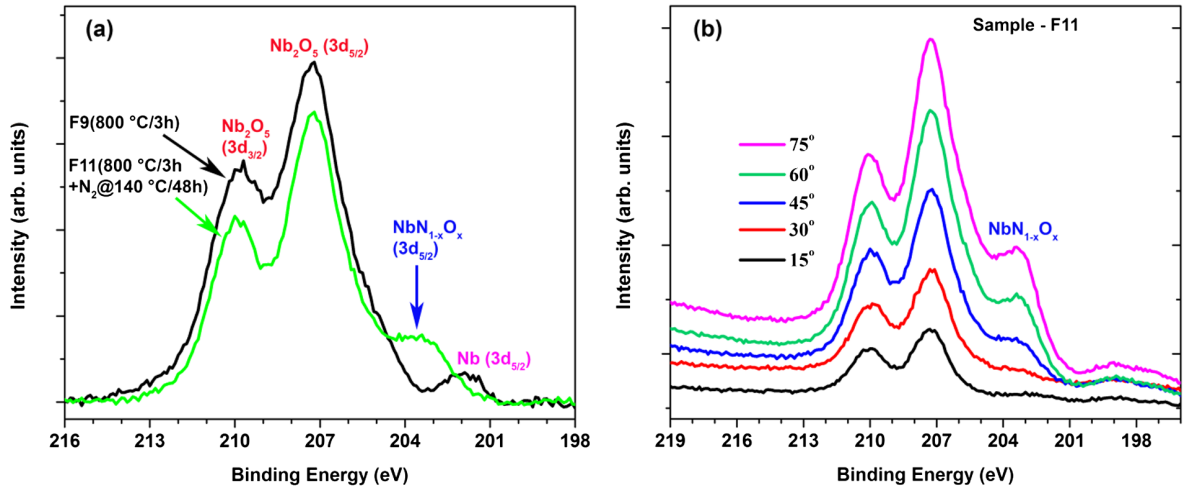

FIG. 6. (a) Background subtracted XPS spectra on sample F9 (800 °C/3 hrs) and F11 (800 °C/3 hrs + 140 °C/48 hrs @ 25 mTorr N_2) at 45° takeoff angle. (b) Angle resolved XPS on sample F11.

increased the signal acquired is from an increased range of depth).

Figure 6 shows the Nb 3d peak for a sample that was heat treated at 800 °C/3 h and 800 °C/3 h with 140 °C N infusion. The peak around 203.2 eV can be interpreted as NbN_x or $NbN_{1-x}O_x$ peak. From the phase diagram of Nb-N, NbN is not thermodynamically favorable to occur below 400 °C, hence we interpret this peak mainly as a $NbN_{(1-x)}O_x$ peak. Also the Nb peak at 202 eV is absent in the nitrogen infused sample indicating that the $NbN_{1-x}O_x$ layer is sufficiently thick that the photoelectrons from the underlying Nb do not reach the surface. Furthermore, the Nb-3d peak intensities increase with takeoff angle due to increased signal to noise ratio from the subsurface. At the lowest takeoff angle only the Nb_2O_5 peak is apparent. The $NbN_{1-x}O_x$ peak shows up only around 45 degrees takeoff angle. This suggests that the surface of the low temperature nitrogen infused samples have a protective oxide layer, below which the oxynitrides layer is present with a thickness greater than 10 nm.

C. TOF-SIMS results

TOF-SIMS analyses [22] were conducted using a TOF SIMS V (ION TOF, Inc. Chestnut Ridge, NY) instrument equipped with a Bi_n^{m+} (n = 1–5, m = 1, 2) liquid metal ion gun, Cs^+ sputtering gun and electron flood gun for charge compensation. Both the Bi and Cs ion columns are oriented at 45° with respect to the sample surface normal. The instrument vacuum system consists of a load lock for rapid sample loading and an analysis chamber, separated by the gate valve. The analysis chamber pressure is maintained below 5.0×10^{-9} mbar to avoid contamination of the surfaces to be analyzed. For the depth profiles acquired in this study, 3 keV low energy Cs^+ with 20 nA current was used to create a 120 μm by 120 μm area, and the middle 50 μm by 50 μm area was analyzed using about 0.3 pA Bi_3^+ primary ion beam. The negative secondary ion mass spectra were calibrated using H^-, O^-, Nb^-, and NbO^-. The positive secondary ion mass spectra were calibrated using H^+, Nb^+, $CsNb^+$ and Cs_2Nb^+. The concentrations were calculated using standard C, N and O implant into standard niobium. Figure 7 shows the concentration of C^-, O^- and NbN^- on samples F9–12. Since nitrogen does not have a significant negative secondary ion yield in SIMS,

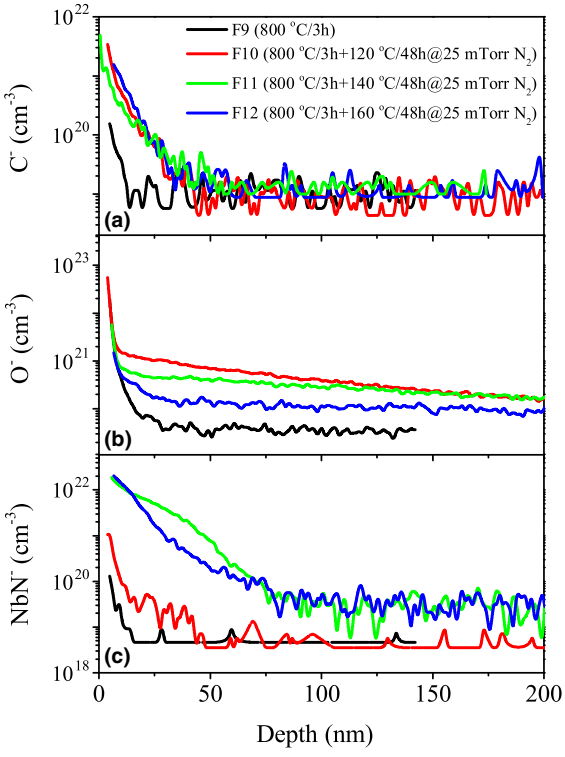

FIG. 7. SIMS depth profile of (a) carbon, (b) oxygen and (c) nitrogen measured in samples F9–F12.

NbN^- ions were used to monitor the N signal. As expected, sample F9 showed the lowest concentrations of O, C and N within rf penetration depth and elemental concentration increases when nitrogen is injected during the furnace treatment. The concentration of oxygen increased with decreasing baking temperature: this could be due to the absorption of residual oxygen from the furnace, from residual water vapor in the gas injection lines, or from residual oxygen from the nitrogen gas cylinder. The higher concentration of NbN^- observed in samples F11 and F12 indicates the diffusion of nitrogen within ~50 nm from the surface, which is consistent with the diffusion coefficient for N into Nb at 160 °C being 6.02×10^{-25} m^2/s [23], resulting in a diffusion depth of 46 nm after 48 h. The NbN^- concentration at a depth of ~10–50 nm from the surface is ~1–10 at.%.

SIMS analysis of a Nb sample annealed at 800 °C for 10 h, 160 °C for 48 h with nitrogen and 160 °C for 168 h, reported in Ref. [24], showed oxygen and carbon concentrations within the top ~100 nm to be more than 1 order of magnitude higher than that of nitrogen. Although our data show higher concentration of O and C at the surface after annealing at 800 °C/3 h, 160 °C/48 h with nitrogen, than after annealing at 800 °C/3 h without nitrogen, the diffusion depth of O and C is limited to ~20 nm and their concentration is comparable to that of N within this depth. It should be noticed that the annealing parameters of the sample in Ref. [24] are different than the ones used in our study and the nitrogen partial pressure during the 160 °C/48 h baking is not specified in Ref. [24]. Differences in the purity of the gas and the cleanliness of the gas injection lines could also explain the difference between the SIMS data of Ref. [24] and those shown in Fig. 7.

Figure 8 showed the ratio of counts/s for H^- and Nb^- for samples F9–F12. Surprisingly, the hydrogen concentration

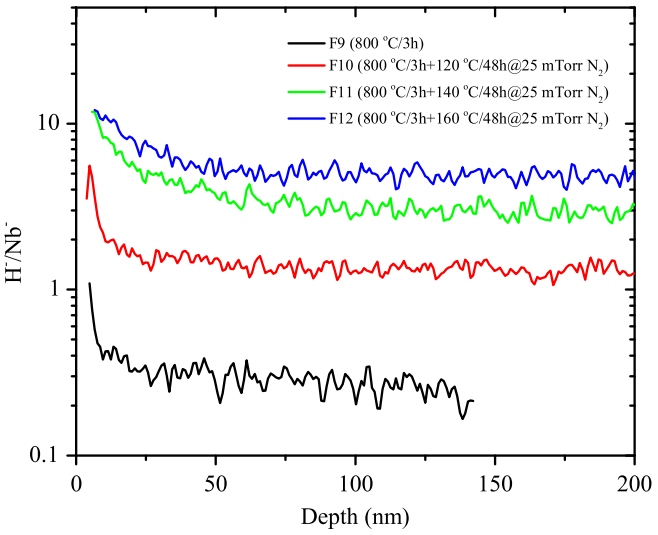

FIG. 8. H^-/Nb^- as a function of depth measured by TOF-SIMS in Nb samples F9–F12.

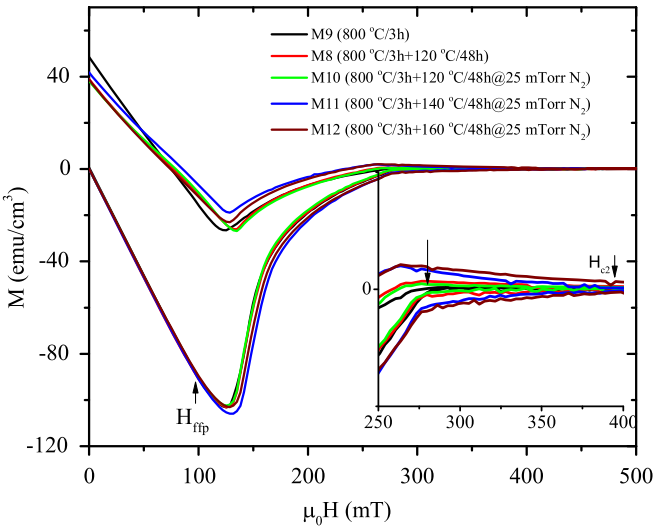

FIG. 9. Isothermal dc magnetic hysteresis of samples M8–M12 measured at 4.2 K. The inset shows the $M(H)$ close to H_{c2} showing an enhanced H_{c2} for samples M11 and M12.

increased with increasing baking temperature. This increase may be due to either the reabsorption of hydrogen in the sample during the cooldown of the cavity from 800 °C or the trapping of the hydrogen near surface due to the introduction of nitrogen. Additional SEM measurements on cross-sectional areas of the samples are planned to further investigate the presence of hydrides close to the surface.

D. First flux penetration by dc magnetization

The dc magnetization measurements were acquired with the 5 T quantum design superconducting quantum interference device system. Cylindrical samples were first zero field cooled to 4.2 K and then the dc magnetization measurements were made by applying a dc field parallel to the length direction of the samples. Figure 9 shows the isothermal dc magnetic hysteresis of samples M8–M12 measured at 4.2 K. No significant change in bulk pinning and field of first flux penetration (H_{ffp}) was observed after low temperature nitrogen infusion. However, higher H_{c2} values were obtained in samples M11 and M12 as shown in the inset of Fig. 9.

V. DISCUSSION

The rf measurements on the treated SRF cavity and the surface analyses of the sample coupons showed that the heat treatment on SRF cavities at low temperature (120–160 °C) significantly alters the rf surface and hence the rf performance. Low temperature (100–150 °C) baking under ultrahigh vacuum has been the standard practice for the final preparation of SRF cavities in order to recover from the high field Q-slope. The improvement in high field Q-slope with increase in accelerating gradient

was explained as the result of oxygen diffusion in the bulk of the cavity [25] or due to the strong suppression of hydride precipitation caused by the change in concentration of vacancy-hydrogen complexes [26]. A comprehensive model capable of explaining all of the experimental results related to the high field Q-slope and baking effect is still lacking. Very limited data regarding the high-field behavior of cavities treated by the high-temperature nitrogen doping followed by EP, mainly because of the reduced quench field, typically <100 mT, above which the high-field Q-slope typically occurs in BCP or EP treated cavities.

An important outstanding issue to increase the quality factor at or below 2 K is the increase in residual surface resistance, which is typically observed after the standard low temperature baking in UHV. Contributions to the residual resistance could come from the presence of "defects" such as damaged layers, metallic suboxides, subgap states, dielectric losses, and trapped magnetic field.

XPS measurements indicate that the outermost dielectric Nb_2O_5 layer decomposes into metallic suboxides such as NbO_x (x = 0.5–2) while baking at 120 °C in UHV [27–29]. However, subsequent exposure of the Nb surface to air reoxidizes the surface increasing the thickness of the Nb_2O_5 layer at the expenses of the suboxides [30]. Radio frequency measurements on cavities for which the oxide layer was stripped by rinsing with HF and regrown after exposure to air and water, following the low-temperature UHV baking show that the residual resistance is reduced back to values similar to those prior to baking [31].

For the study reported in this article, the Nb_2O_5 is dissolved by the annealing at 800 °C and perhaps only few monolayers of NbO_x might be on the cavity surface once the temperature dropped to <300 °C, at which point N_2 is injected into the furnace. A niobium oxynitrite layer might be formed on the surface during baking at 120–160 °C in nitrogen atmosphere and subsequent exposure of the surface to air and water promotes the growth of the outermost Nb_2O_5 layer. The XPS results indicate that an $NbN_{1-x}O_x$ layer is still present between the Nb_2O_5 layer and the bulk Nb. The electronic properties of such a layer and their influence on the electronic density of states of the adjacent superconducting Nb might explain the difference in the rf performance of "nitrogen infused" cavities compared to those which were subjected to the standard UHV baking. It is also possible that the injection of nitrogen at 290 °C could initiate the growth of nanoscale normal-conducting niobium nitride islands, which could be the surface features mentioned in Sec. IV A. An increase in the density or size of such normal-conducting features with increasing infusion temperature might explain the quench field behavior.

A theoretical model in which the surface resistance of a superconductor coated with a thin normal metal was recently presented and showed that the $R_s(B_p)$ behavior observed in SRF cavities following different surface preparations can be explained with changes in the thickness of the normal layer and of the interface boundary resistance [32]. A recent theoretical model proposed by Gurevich extends the zero-field BCS surface resistance to high rf fields, in the dirty limit [33]. Such a model calculates $R_s(H)$ from the nonlinear quasiparticle conductivity $\sigma_1(H)$, which requires knowledge of the quasiparticles' distribution function. The calculation was done for two cases, one which assumes the equilibrium Fermi-Dirac distribution function and one for a nonequilibrium frozen density of quasiparticles. A nonequilibrium distribution function is appropriate when the rf period is shorter than the quasiparticles' relaxation time. $R_s(H)$ is calculated numerically for these two cases and it depends on a single parameter, α, which is related to the heat transfer across the cavity wall, the Nb-He interface and between quasiparticles and phonons.

Figure 10 shows the measured $R_s(B_p)$ after N-infusion at 140 and 160 °C, normalized to the value at B_p~10 mT, along with the curves calculated with the model of Ref. [33]. The data after N-infusion at 120 °C do not show any Q-rise and therefore cannot be described with the model. Good agreement with the experimental data up to B_p~130 mT is obtained with $\alpha = 0.08$ and the equilibrium distribution function for the N-infusion at 140 °C and with $\alpha = 1.125$ and the nonequilibrium distribution function for the N-infusion at 160 °C.

A qualitative interpretation from using Gurevich's model to describe our data is that the increase of the N-infusion temperature from 140 to 160 °C results in increase of the quasiparticles' relaxation time, which becomes longer than the rf period after the infusion at 160 °C. A high density of subgap states, which are not considered in Gurevich's theory, would completely suppress the Q-rise phenomenon, as observed after infusion at 120 °C, and would reduce the

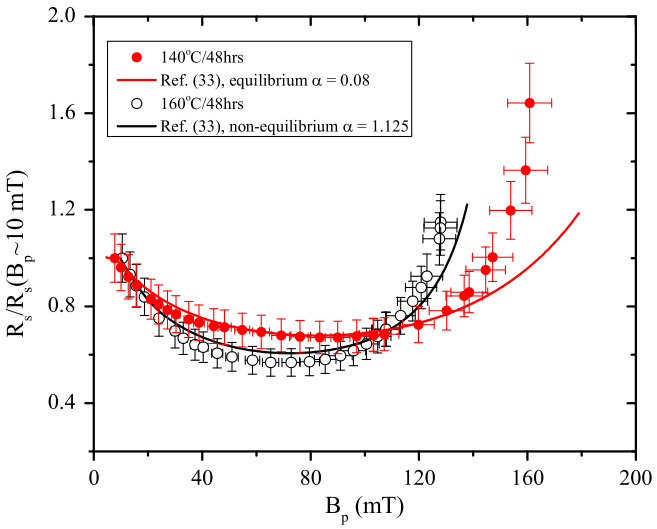

FIG. 10. $R_s/R_s(B_p \sim 10\ \text{mT})$ vs B_p calculated using the model in Ref. [33] along with the experimental data for cavity heat treated at 140 and 160 °C, respectively.

quasiparticles' relaxation time. Therefore, we may interpret our cavity test results as being related to a decreasing density of subgap states as the N-infusion temperature is increased from 120 to 160 °C.

Unlike the rf properties, the dc magnetization measurements showed no significant change on the bulk superconducting properties as a result of low temperature nitrogen infusion. The hysteresis loop observed in the magnetization data showed no change in the bulk magnetic flux pinning. A closer look near H_{c2} (Fig. 6 inset) for samples M11 and M12 showed enhanced H_{c2} values, probably due to the surface barrier effect [34,35] as a result of samples being treated at higher temperatures (140–160 °C) in nitrogen.

VI. CONCLUSION

Improvement in the quality factor of an SRF Nb cavity was observed after annealing at 800 °C/3 h in vacuum followed by baking at 120–140 °C in low partial pressure of nitrogen inside a furnace ("N-infusion"), with a modest ~14% degradation of the maximum accelerating gradient, compared to the quench field after 120 °C bake in UHV. A larger reduction (~35%) of the quench field was observed when the baking temperature was 160 °C but with a pronounced increase of the quality factor with field, similar to that observed in cavities treated by high temperature nitrogen doping followed by electropolishing.

SEM analysis of sample coupons showed the presence of surface features after N-infusion, which might be nanoscale nitrides, and XPS analysis showed the presence of a possible niobium oxynitrate layer at the surface. Impurities depth profiling by TOF-SIMS showed a diffusion profile for nitrogen in Nb down to ~50 nm and higher H concentration after N-infusion. Further studies are ongoing to better identify and understand the role of impurities and precipitates on the cavity performance.

A comparison of the field dependence of the surface resistance after N-infusion with a recent theoretical model that extends the calculation of the BCS surface resistance to high rf fields suggests an increase in the quasiparticles' relaxation time with increasing infusion temperature, which could be due to a decreasing density of subgap states. No significant changes of bulk critical fields or pinning properties seem to occur by N-infusion.

Overall, a quality factor as high as $\sim 2 \times 10^{10}$ at 1.5 GHz was achieved at a gradient of 35 MV/m by 800 °C annealing and N-infusion at 140 °C. Such performance would be of great interest for lowering the cryogenic heat load of high-energy accelerators such as the proposed Linear Collider [36].

ACKNOWLEDGMENTS

We would like to acknowledge Jefferson Lab technical staff for the cavity surface processing and cryogenic support and Dr. Elaine Zhou at Analytical Instrumentation Facility (AIF), North Carolina State University, for SIMS measurements. We would like to acknowledge Professor A. Gurevich from Old Dominion University for useful discussions and providing the code to calculate the field dependence of the surface resistance. We would also like to acknowledge A. Palczewski from Jefferson Lab for helpful discussions. The work done at Florida State University is supported by the U.S. Department of Energy, Office of Science, Office of High Energy Physics under Awards No. DE-SC 0009960 (FSU) and No. DE-FG02-09ER41638 (MSU) and the State of Florida. Additional support for the National High Magnetic Field Laboratory facilities is from the NSF: NSF-DMR-1157490. This manuscript has been authored by Jefferson Science Associates, LLC under U.S. DOE Contract No. DE-AC05-06OR23177.

[1] P. Dhakal, G. Ciovati, and G. R. Myneni, A path to higher Q_0 in large grain niobium cavities, in *Proceedings of the 3rd International Particle Accelerator Conference, New Orleans, LA, 2012*, edited by Jacow (IEEE, Piscataway, NJ, 2012) p. 2426, (www.jacow.org).

[2] P. Dhakal *et al.*, Effect of high temperature heat treatments on the quality factor of a large-grain superconducting radio-frequency niobium cavity, Phys. Rev. ST Accel. Beams **16**, 042001 (2013).

[3] P. Dhakal, G. Ciovati, P. Kneisel, and G. R. Myneni, Enhancement in quality factor of SRF niobium cavities by material diffusion, IEEE Trans. Appl. Supercond. **25**, 1 (2015).

[4] A. Grassellino, A. Romanenko, D. Sergatskov, O. Melnychuk, Y. Trenikhina, A. Crawford, A. Rowe, M. Wong, T. Khabiboulline, and F. Barkov, Nitrogen and argon doping of niobium for superconducting radio frequency cavities: A pathway to highly efficient accelerating structures, Supercond. Sci. Technol. **26**, 102001 (2013).

[5] G. Pfeifer and H. Wipf, The trapping of hydrogen in niobium by nitrogen interstitials, J. Phys. F **6**, 167 (1976).

[6] D. Richter, R. J. Rush, and J. M. Rowe, Localized modes and hydrogen trapping in niobium with substitutional impurities, Phys. Rev. B **27**, 6227 (1983).

[7] S. Balachandran, S. Chetri, P. Dhakal, D. Larbalestier, and P. J. Lee, Hydrogen and hydride precipitation in SRF Nb revealed by *ex situ* metallographic technique, in SRF'17, Lanzhou, China, 2017.

[8] G. Ciovati, P. Dhakal, and A. Gurevich, Decrease of the surface resistance in superconducting niobium resonator cavities by the microwave field, Appl. Phys. Lett. **104**, 092601 (2014).

[9] A. Gurevich, Reduction of Dissipative Nonlinear Conductivity of Superconductors by Static and Microwave Magnetic Fields, Phys. Rev. Lett. **113**, 087001 (2014).

[10] D. Gonnella, R. Eichhorn, F. Furuta, M. Ge, T. Gruber, G. Hoffstaetter, J. Kaufman, P. N. Koufalis, J. T. Maniscalco, and M. Liepe, Improved N-doping protocols for SRF

cavities, in *Proceedings of IPAC'16, Busan, Korea*, edited by Jacow Collaboration (2016), p. 2323 (www.jacow.org).

[11] S. Chetri, D. C. Larbalestier, P. J. Lee, Z. H. Sung, and P. Dhakal, Determination of bulk and surface superconducting properties of N2-doped cold worked, heat treated and electropolished SRF grade niobium, in *Proceedings of SRF 2015, Whistler, BC, Canada*, edited by Jacow Collaboration (www.jacow.org) (2015), p. MOPB052.

[12] M. Checchin, A. Grassellino, M. Martinello, S. Posen, A. Romanenko, and J. F. Zasadzinski, Ultimate gradient limitation in niobium superconducting accelerating cavities, in *Proceedings of IPAC 2016, Busan, Korea*, edited by Jacow Collaboration (www.jacow.org) (2016), p. 2254.

[13] G. Ciovati, G. Myneni, F. Stevie, P. Maheshwari, and D. Griffis, High field Q slope and the baking effect: Review of recent experimental results and new data on Nb heat treatments, Phys. Rev. ST Accel. Beams **13**, 022002 (2010).

[14] P. Dhakal, G. Ciovati, and G. R. Myneni, Analysis of post-wet-chemistry heat treatment effects on Nb SRF surface resistance, in, *Proceedings of SRF'13, Paris, France*, edited by Jacow Collaboration (www.jacow.org) (2013), p. 414.

[15] A. Grassellino *et al.*, Unprecedented quality factors at accelerating gradients up to 45 MV m^{-1} in niobium superconducting resonators via low temperature nitrogen infusion, Supercond. Sci. Technol. **30**, 094004 (2017).

[16] P. N. Koufalis, F. Furuta, M. Ge, D. Gonnella, J. J. Kaufman, M. Liepe, J. T. Maniscalco, and R. D. Porter, Low temperature nitrogen baking of Q_0 SRF cavities, in *Proceedings of LINAC2016, East Lansing MI*, edited by Jacow Collaboration (www.jacow.org) (2016), p. 472.

[17] A. D. Palczewski, M. Kelly, J Tuggle, and C. E. Reece, Investigation of nitrogen absorption and nitride growth of SRF cavity grade RRR niobium as a function of furnace temperature, in *Proceedings of LINAC 2016, East Lansing, MI*, edited by Jacow Collaboration (www.jacow.org) (2016), THOP02.

[18] S. Posen, M. Checchin, A. C. Crawford, A. Grassellino, M. Martinello, O. S. Melnychuk, A. Romanenko, D. A. Sergatskov, and Y. Trenikhina, Efficient expulsion of magnetic flux in superconducting radiofrequency cavities for high Q_0 applications, J. Appl. Phys. **119**, 213903 (2016).

[19] D. C. Mattis and J. Bardeen, Theory of the anomalous skin effect in normal and superconducting metals, Phys. Rev. **111**, 412 (1958).

[20] J. Halbritter, Karlsruhe Nuclear Research Center External Report No. 3/70-6, 1970.

[21] G. Ciovati, Effect of low-temperature baking on the radio-frequency properties of niobium superconducting cavities for particle accelerators, J. Appl. Phys. **96**, 1591 (2004).

[22] A. M. Belu, D. J. Graham, and D. G. Castner, Time-of-flight secondary ion mass spectrometry: Techniques and applications for the characterization of biomaterial surfaces, Biomaterials **24**, 3635 (2003).

[23] R. J. Farraro and R. B. McLellan, Diffusion of nitrogen in vanadium and niobium, Mater. Sci. Eng. **33**, 113 (1978).

[24] P. N. Koufalis, D. L. Hall, M. Liepe, and J. T. Maniscalco, Effect of interstitial oxygen and carbon on niobium superconducting cavities, arXiv:1612.08291v2.

[25] G. Ciovati, Improved oxygen diffusion model to explain the effect of low-temperature baking on high field losses in niobium superconducting cavities, Appl. Phys. Lett. **89**, 022507 (2006).

[26] A. Romanenko, F. Barkov, L. D. Cooley, and A. Grassellino, Proximity breakdown of hydrides in superconducting niobium cavities, Supercond. Sci. Technol. **26**, 035003 (2013).

[27] Q. Ma and R. A. Rosenberg, Angle-resolved x-ray photoelectron spectroscopy study of the oxides on Nb surfaces for superconducting rf cavity applications, Appl. Surf. Sci. **206**, 209 (2003).

[28] A. Dacca, G. Gemme, L. Mattera, and R. Parodi, XPS analysis of the surface composition of niobium for superconducting rf cavities, Appl. Surf. Sci. **126**, 219 (1998).

[29] K. Kowalski, A. Bernasik, W. Singer, X. Singer, and J. Camra, *In situ* XPS investigation of the baking effect on the surface oxide structure formed on niobium sheets used for superconducting rf cavity production, in *Proceedings of SRF'03, Lubeck/Travemunde, Germany*, edited by Jacow Collaboration (www.jacow.org) (2003), p. 610.

[30] H. Tian, B. Xiao, M. J. Kelley, C. Reece, A. DeMasi, L. Pipe, and K. E. Smith, Recent XPS studies of the effect of processing on Nb SRF surfaces, in *Proceedings of SRF'07, Beijing, China*, edited by Jacow Collaboration (www.jacow.org) (2007), p. 158.

[31] A. Romanenko, A. Grassellino, F. Barkov, and J. P. Ozelies, Effect of mild baking on superconducting niobium cavities investigated by sequential nanoremoval, Phys. Rev. ST Accel. Beams **16**, 012001 (2013).

[32] A. Gurevich and T. Kubo, Surface impedance and optimum surface resistance of a superconductor with imperfect surface, Phys. Rev. B **96**, 184515 (2017).

[33] A. Gurevich, Theory of rf superconductivity for resonant cavities, Supercond. Sci. Technol. **30**, 034004 (2017).

[34] J. Clem, Flux-line-cutting threshold in type II superconductors, in *Proceedings of Low Temperature Physics LT 13*, edited by K. D. Timmerhaus *et al.* (Plenum, New York, 1974), Vol. 3, p. 102.

[35] P. K. Mishra, G. Ravikumar, V. C. Sahni, M. R. Koblischka, and A. K. Grover, Surface pinning in niobium and a high-Tc superconductor, Physica (Amsterdam) **269C**, 71 (1996).

[36] L. Evans and S. Michizano, The international linear collider machine staging report 2017, arXiv:1711.00568.